Journal of Magnetic Resonance 198 (2009) 146–150

Contents lists available at ScienceDirect

Journal of Magnetic Resonance

journal homepage: www.elsevier.com/locate/jmr

MRI profiles over very wide concentration ranges: Application to swelling of a bentonite clay

S.V. Dvinskikh *, K. Szutkowski [1], I. Furó

Division of Physical Chemistry, Department of Chemistry, Royal Institute of Technology, Teknikringen 36, SE-10044 Stockholm, Sweden

ARTICLE INFO

Article history:
Received 24 November 2008
Revised 27 January 2009
Available online 4 February 2009

Keywords:
MRI
Clay
Bentonite
Montmorillonite
Environmental science and technology

ABSTRACT

In MRI investigation of soils, clays, and rocks, mainly mobile water is detected, similarly to that in biological and medical samples. However, the spin relaxation properties of water in these materials and/or low water concentration may make it difficult to use standard MRI approaches. Despite these limitations, one can combine MRI techniques developed for solid and liquid states and use independent information on relaxation properties of water, interacting with the material of interest, to obtain true images of both water and material content. We present procedures for obtaining such true density maps and demonstrate their use for studying the swelling of bentonite clay by water. A constant time imaging protocol provides 1D mapping of the clay distribution in regions with clay concentration above 10 vol%. T_1 relaxation time imaging is employed to monitor the clay content down to 10^{-3} vol%. Data provided by those two approaches are in good agreement in the overlapping range of concentrations. Covering five orders of magnitude of clay concentration, swelling of sodium-exchanged bentonite clays from pre-compacted pellets into a gel phase is followed in detail.

1. Introduction

While most magnetic resonance imaging (MRI) applications concern medical research, there is a rapidly increasing number of MRI studies in the field of environmental science and technology [1,2]. In MRI investigation of, e.g., soils, clays, and rocks, mainly water signal is detected, similarly to MRI of biological and medical samples. However, a strong variation of water mobility and a wide spread of water spin relaxation properties in these materials make it difficult to use standard MRI approaches. Despite these limitations, we show below that one can combine MRI techniques developed for solid and liquid states and use independent information on relaxation properties of water, interacting with the material of interest, to obtain true images of both water and material distribution in a wide range of concentrations.

Compacted bentonite clay is currently attracting a lot of attention as a promising "self-sealing" buffer material to build in-ground barriers for the encapsulation of radioactive waste. It is expected to fill up the space between waste canister and surrounding ground by swelling and thus delay water flow and migration between the host rock and the canister. Evaluation and understanding of the swelling properties of pre-compacted bentonite are of uttermost importance for designing such buffers. Our goal in the present study was to develop an MRI approach that is suitable for monitoring quantitatively the spatial distribution of clay in water and thereby to follow the swelling kinetics of pre-compacted clay material in contact with a water reservoir. Since these types of systems evolve from essentially solid state to dilute and highly mobile gel and sol phases the clay concentration range of interest may span several orders of magnitude. Corresponding variation by orders of magnitude of relaxation times may complicate the interpretation of images by inducing a strong relaxation contrast. Here, we turn this complication into an advantage and combine different MRI techniques and relaxation time measurements for obtaining clay concentration profiles that cover an unprecedented concentration range of five orders of magnitude.

Previously, NMR has extensively been used for investigations of spectroscopic and spin relaxation properties of dry bentonite and bentonite/water mixtures at equilibrium [3–9]. Water self-diffusion [8,9] and its anisotropy [10,11] in clay suspensions have also been studied. We also note that MRI has been previously applied to observe the kinetics of moisture gradient in a bentonite clay in contact with water reservoir [12], albeit in a much narrower range of accessed clay concentrations.

2. Experimental

MRI experiments were performed on a Bruker Avance II 300 MHz spectrometer. To acquire 1D images of samples at high

* Corresponding author. Fax: +46 8 790 82 07.
E-mail address: sergey@physchem.kth.se (S.V. Dvinskikh).
[1] Present address: Faculty of physics, Adam Mickiewicz University, Umultowska 85, PL-61614 Poznan, Poland.

1090-7807/$ - see front matter © 2009 Elsevier Inc. All rights reserved.
doi:10.1016/j.jmr.2009.01.035

clay concentration, we used constant time imaging performed on a Bruker Diff25 diffusion probe with 960 G/cm z-gradient. For T_1 relaxation time imaging, a Bruker micro-imaging probe with maximum gradient 150 G/cm and field of view of 25 mm (with gradient homogeneity better than 5%) in three directions was used. To measure vertical profiles up to 80 mm length, the sample was shifted in 20 mm steps.

Purified Na-ion exchanged MX80 clay powder [composition $(Na,Ca)_{0.33}(Al,Mg)_2(Si_4O_{10})(OH)_2{\cdot}nH_2O$, this material is also called bentonite or montmorrilonite] was obtained from Clay Technology AB, Sweden. The material properties of this clay sample are available in detail [13]. Prior to the swelling experiments, the clay was equilibrated at 94% relative humidity over a saturated KNO_3 water solution. The resulting equilibrium water content was estimated to 23 wt% by gravimetric measurements. Disk shaped pellets of 8 mm diameter and 3 mm height were pressed to 1.8 g/cm^3 final density using a pneumatic press and 8 mm die (Lightpath Optical Ltd., UK). The pellets were then fitted tightly at the bottom of a 8 mm i.d. quartz tube. The swelling experiment started by adding deionized water into the tube over the pellet. This resulted in one-dimensional swelling vertically upwards that we intended to follow by 1D MRI experiments.

Clay suspensions for measuring the concentration dependence of the spin relaxation rates were prepared by dispersing dry bentonite in deionized water. The bentonite volume fraction ϕ_b was calculated from the weight fraction w_b using the relationship $\phi_b = w_b/(\rho_b/\rho_w + [1 - \rho_b/\rho_w]w_b)$ with dry solid bentonite and water densities of $\rho_b = 2.7$ g/cm^3 and $\rho_w = 1.0$ g/cm^3, respectively.

3. MRI methodology

One faces a two-pronged challenge when performing MRI experiments in our materials. First, temporal and spatial variation of clay concentration by more than five orders of magnitude leads to a corresponding variation of image intensity. Second, orders of magnitude variation in relaxation times (from milliseconds to seconds for T_1 and from 10^{-5} s to seconds for T_2) induces a strong relaxation contrast in the images.

In our design we assume that the whole sample volume is occupied by clay particles and water which can be macroscopically separated (as at the beginning of the swelling process), or form a nano- and molecular-scale mixture (sol at the end of swelling) or be in a state somewhere in between those two extremes. Possible contribution to the sample volume by trapped air was minimized by sample preparation and was experimentally verified to be negligible during most of the swelling process (see below). Hence, clay volume fraction $\phi_b(z)$ at a particular height z can be obtained from the water fraction $\phi_w(z)$ as $\phi_b(z) \approx 1 - \phi_w(z)$. Because of the involved subtraction, this approach is limited to high (in practice, above a few percents) clay concentrations. The water volume fraction profile $\phi_w(z) = s(z)/ref(z)$ is directly obtained from the water signal intensity profile $s(z)$ and reference signal $ref(z)$ of the tube filled with pure water.

Since at high clay concentration our samples exhibited short T_2 and T_1 times, constant time imaging protocol (CTI) was selected as a technique to obtain the water signal intensity profile $s(z)$. CTI is the method that is least susceptible to relaxation contrast and capable of imaging samples with very short T_2 [14–16]. CTI was employed with spatial resolution set to 0.156 mm and encoding delay $\tau = 8$ μs, limited by the available gradient strength and the dead time of the probe. At high clay content, Gaussian decay of FID signal was observed with a minimum value of 16 μs for the time constant T_2^*. Hence, our raw images were T_2^*-weighted even with the shortest available encoding delay. This effect was corrected for by extrapolating the relation $S(z,\tau) = s(z)\exp[-(\tau/T_2^*)^2]\sin\alpha$ to zero encoding delay; α is the rf flip angle [17,18]. Hence, a series of images were collected with different encoding delays τ and correspondingly adjusted gradient strength to maintain a constant k-space step [19]. The bandwidth of 0.4 μs long rf pulses (yielding $\alpha = 7°$) was sufficient for excitation of the

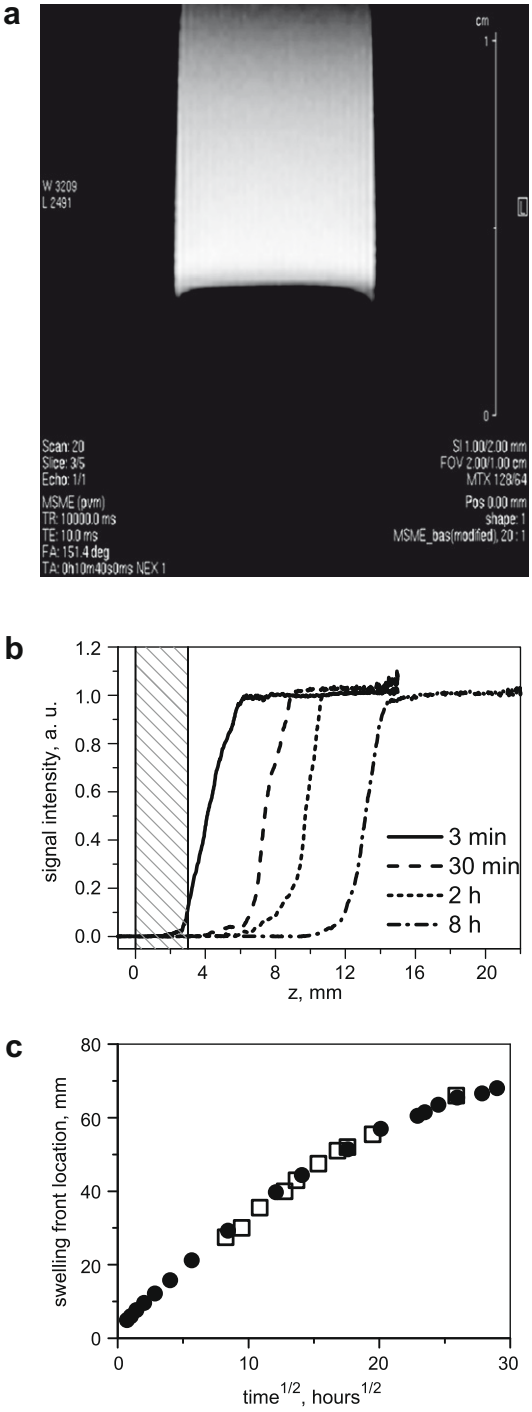

Fig. 1. (a) 2D Image (sagittal cross-section) obtained by a conventional spin-echo-based imaging sequence of the Na-MX80 clay swelling in water. The image is dominantly contributed by free water, while the signal intensity of the water interacting with the clay is strongly attenuated by spin relaxation. (b) 1D vertical profiles acquired at different times after adding water to the clay sample. The shaded area indicates the initial position of clay pellet. (c) The propagation of the swelling front (the gel/water interface) defined by the position of the half-intensity point in (b) (dots) compared to the position of the visually observable interface (squares) between transparent pure water part and the opaque yellowish gel phase.

sample volume. For this small flip angle the repetition time of 1 s was sufficiently long to have negligible influence from longitudinal relaxation with the maximum T_1 time of 3.1 s [16,19], (see also Fig. 3 below). Hence, minimum time required for acquiring an image of 128 spatial points was 2 min.

At clay concentrations at or below a few %, the approach described above was not judged to be sufficiently accurate. Instead, at those concentrations we used relaxation imaging and converted the obtained relaxation rate profiles into concentration profiles via suitable calibration data. Hence, 1D images of water T_1 were recorded using conventional spin-echo imaging combined with inversion recovery. Using an equilibration time of 10 s, maximum relaxation delay of 9 s and 20 delay points, experimental time was limited to approximately 5 min. For conversion, we measured the T_1 time dependence on clay content in homogeneous clay suspensions of different concentrations.

The consistency of the combination of these two approaches had to be tested. A suitable test was provided by comparing the obtained clay contents in the overlapping region of concentrations (see below). This overlap region was 4–12 vol% of clay set, respectively, by the lower and upper limits of the direct CTI and relaxation imaging methods.

4. Results and discussion

4.1. Qualitative observation of clay swelling in water by MRI

4.1.1. Images of free water

With conventional spin-echo-based imaging sequences, water images of the swelling clay exhibited significant relaxation contrast because the water signal from within the clay was strongly attenuated during the echo delay. Examples of ^{1}H 2D and 1D conventional spin-echo images, shown in Fig. 1a and b, respectively, illustrate that the obtained images are mainly contributed by free water. Hence, we observed the interface between water and the swelling clay as a sharp cut. Therefore, conventional spin-echo-based imaging informs primarily on the propagation of the swelling front (Fig. 1c) as verified by the coincidence of the image intensity drop with the visually observable interface between the transparent water column and the opaque yellowish gel phase. Spatial clay distribution cannot, however, be obtained from this kind of experiment.

4.1.2. Images of confined water

At short swelling times, the behavior of pre-compacted bentonite in water can be most simply visualized in conventional experiments if one adds heavy water. In this case, the ^{1}H signal originates solely from the water initially present in the water-presaturated clay. Examples of T_2-corrected one-dimensional CTI profiles are shown in Fig. 2. Unfortunately, water diffusion in bentonite clay is rapid even at low water content ($D \sim 10^{-9}$ m^2/s at 20–30 weight% of water [8,12]). Hence, on the significant time scale of hours the diffusion path length of water molecules $\langle r^2 \rangle^{1/2} = (2Dt)^{1/2} \approx 3$ mm becomes comparable to the pellet size which renders this type of experiment not quantitative as concerning the clay distribution.

4.2. Quantitative characterization of the swelling process

MRI experiments described above provided a simple tool to qualitatively follow the swelling process and estimate its temporal and spatial scale. To obtain a quantitative image of the clay spatial distribution and its time evolution a more elaborate approach is required as described above in Section 3.

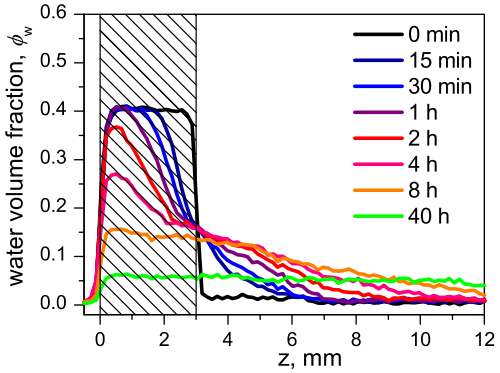

Fig. 2. ^{1}H one-dimensional profiles of Na-MX80 clay swelling in D_2O in vertical tube. Signal is contributed by the water molecules originally present in the clay containing 23 weight% (corresponding to 41 vol%) of water. Water volume fraction ϕ_w is calculated by normalizing the signal intensity of the swelling clay sample to the signal of the tube filled with pure H_2O. The shaded area indicates the initial position of the clay pellet.

4.2.1. Low clay concentration region: relaxation time imaging

Spin relaxation times provide very sensitive probes of the bentonite content in clay/water suspensions [8,9,20]. Hence, clay density maps can be acquired using T_1-imaging techniques if there exists a monotonic calibration function that relates T_1 times to clay content. To obtain such a calibration function, the relaxation rates were measured for clay concentrations up to 20 vol% as presented in Fig. 3. Single exponential relaxation behavior is commonly observed for these types of clays in gel and sol phase and is indicative of fast exchange between bulk and interlayer water [8,9,21]. In the measured region, the concentration dependence of the longitudinal relaxation rate $R_1 = 1/T_1$ can be approximated by a linear function, as shown in Fig. 3 by the fit for the $R(\phi_b) = R_1(\phi_b) - R_1(0)$, where $R_1(0) = 0.32$ s^{-1} is the relaxation rate of pure water. In practice, the range of concentration accessible by T_1-imaging is limited to maximum ≈ 12 vol% by the decrease of T_2 times with the increase of clay content. When applying the calibration data of Fig. 3, it is assumed that T_1 times obtained for equilibrium samples are also relevant for an expanding clay sample (local equilibrium).

Relaxation rate profiles $R(z)$ for a swelling Na-MX80 clay are shown in Fig. 4a. Full sample profiles (that is, down to the bottom of the tube) were obtained only at long swelling times exceeding 100 h. At shorter times and at distances <5 mm from the bottom of the tube, higher clay concentration resulted in short $T2$ times (<100 μs) that precluded spin-echo-type experiments. The linear

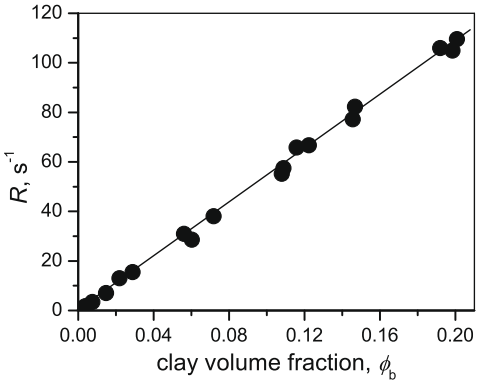

Fig. 3. The concentration dependence of $R = R_1 - R_1(0)$ where R_1 is longitudinal relaxation rate of water in homogeneous aqueous dispersions of Na-MX80 clay and $R_1(0) = 3.1^{-1}$ s^{-1} is the relaxation rate of pure water. The line is linear best fit with zero intercept.

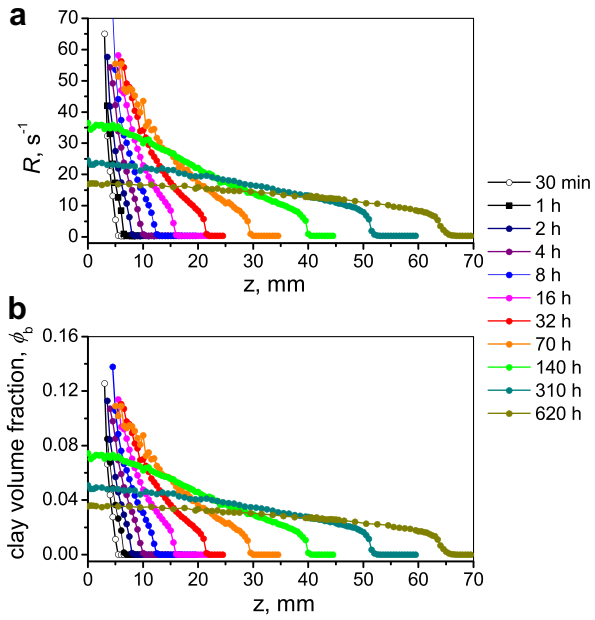

Fig. 4. Relaxation rate (a) and clay volume fraction (b) profiles in a Na-MX80/water sample at different swelling times. Position $z = 0$ corresponds to the bottom of pellet (coinciding with the bottom of the tube).

calibration function as obtained by linear fit to the experimental points in Fig. 3 was then applied to convert relaxation rates to clay volume fractions as shown in Fig. 4b.

4.2.2. High concentration region: direct imaging of water content by CTI

Clay volume fraction profiles $\phi_b(z)$ obtained at different swelling times are shown in Fig. 5. CTI protocol and extrapolation of image intensities to zero dephasing time was employed as described in Section 3. In general, the quantity $\phi_b(z) = 1 - \phi_w(z)$ should be ascribed to the combined volume occupied by the clay particles and air filling the possible voids in the sample. With the present sample density of 1.8 g/cm^3, water content of 23 wt% and density of dry clay particles of 2.7 g/cm^3 air fraction is estimated to be below 7 vol%. Hence, the initial clay fraction in Fig. 5 is likely to be slightly overestimated within this limit. At longer swelling times, as the viscosity drops, it is reasonable to assume that the air escapes and the intensity profile correctly provides the clay content distribution profile.

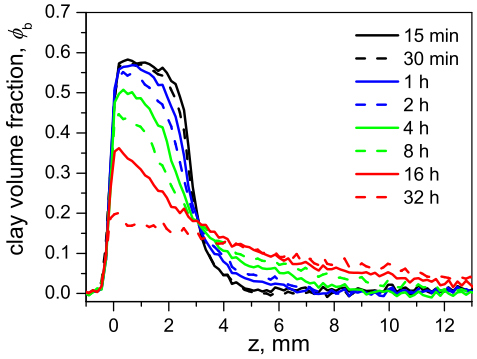

Fig. 5. Clay volume fraction profiles $\phi_b(z) \approx 1 - \phi_w(z)$ in a Na-MX80/water sample at different swelling times as obtained by CTI.

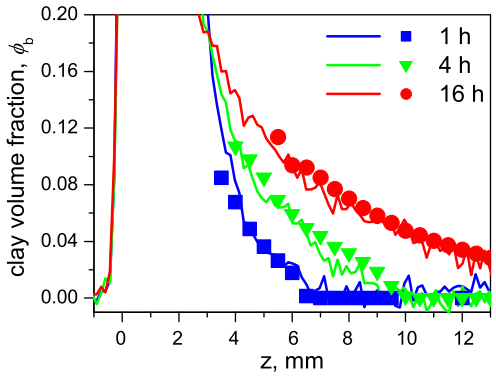

Fig. 6. Comparison of clay volume fraction profiles obtained by CTI (lines) and T_1-imaging (symbols) methods.

4.2.3. Comparing and combining of CTI and relaxation time imaging

Combination of the two techniques described above provides us with the opportunity to measure the clay content over a range spanning five orders of magnitude: starting from solid clay and going to dilute and highly mobile gel and sol phases. Direct imaging of water content by CTI has a practical lower limit for measuring clay content that, in our samples, was about 4 vol%. This lower limit is set by the signal-to-noise level achievable at reasonable experimental times, by possible systematic errors in the reference water profile originating from the variation of the dielectric and magnetic properties of samples during swelling, and by instrumental stability. On the other hand, the accessible range of the relaxation imaging method extends up to approximately 10–12 vol% of clay and is limited by the fast transverse relaxation in concentrated samples. Hence, there exists a significant overlap between the two approaches and this overlap can be straightforwardly exploited for testing the consistency of the two sorts of data. In Fig. 6, the results by the two methods are compared in the relevant concentration range. Clearly, the data are in good agreement.

By combining the results of both techniques the profiles of clay volume fraction covering five orders of magnitude are thus obtained. To properly visualize the full span, data are shown in Fig. 7 on a double logarithmic scale. One interesting and by direct imaging inaccessible feature is the sharp transition from gel phase to pure water. Some additional, but apparently small, averaging of the clay distribution at the gel-water interface in 1D projection

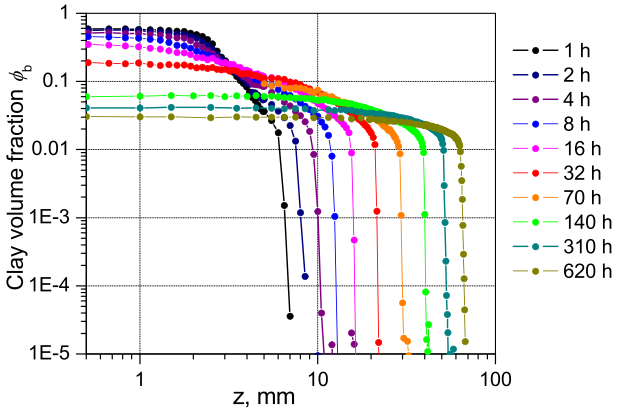

Fig. 7. Profiles of the clay volume fraction in a Na-MX80/water sample at different swelling times. Combined data obtained by CTI and T_1-imaging depict clay distribution in the volume fraction range from 10^{-3}% to 60%.

images was resulted from the meniscus seen in Fig. 1a. Clay fraction at the transition point amounts to ≈1.5 vol% and is practically constant during the swelling process. Even at the longest swelling times there exists a residual concentration gradient (more clearly visible on the linear scale in Fig. 4b). This might be partly attributed to the gravity effect which inhibits achieving the homogeneous clay distribution in the gel phase for swelling in a vertical tube. Further investigations in cells with horizontal and downwards swelling are under way which would clarify the impact of gravity on clay distribution.

5. Conclusion

MRI was applied to monitor the spatial distribution of the clay particles during swelling of bentonite in water. With the conventional ^{1}H spin-echo-based imaging sequence, the signal of free water located above the swelling clay dominates the image because the signal of water interacting with the clay is strongly attenuated by rapid transverse relaxation. Instead, we used constant time imaging to acquire the clay distribution profiles at clay concentrations down to 4 vol%. With CTI, we could attain a dephasing time $\tau < 10$ μs which demanded no or only minor image intensity correction to account for fast transverse relaxation. Clay volume fraction was then directly estimated from the difference between a reference image and water-in-clay image. However, because the interesting parameter, the clay volume fraction, appears as a difference our CTI approach was prone to large error at clay concentrations below a few percent.

Instead, accurate concentration profiles at low clay content were obtained using T_1-imaging and by a subsequent transformation of relaxation data to clay density data by a suitable calibration function. This calibration function had to be measured independently in a series of (homogeneous) samples with different clay concentrations. For the present clay samples, the range of concentrations 0.001–100 vol% could be accessed by our combined experimental protocol. With the present setup, spatial and time resolutions were 0.16 mm and 5 min, respectively. Extensions of the methods to the study of 2D radial swelling or swelling in horizontal slit are straightforward.

Our combined experimental protocol has allowed us to acquire the full concentration profiles during swelling of Na-exchanged MX80 clay samples starting from compacted powder and into the dilute gel phase. We note that one could access even lower concentrations by applying T_2 imaging since T_2 relaxation time is more sensitive to clay particle concentration, especially at higher magnetic field. The method we present here was developed under the motivation of using bentonite clays as a buffer medium to build in-ground barriers for the encapsulation of radioactive waste. Nevertheless, the same method could be applied equally well to study other types of materials in other applications as they swell, dissolve, erode, or sediment.

Acknowledgments

This work has been supported by the Swedish Nuclear Fuel and Waste Management Co (SKB) and the Swedish Research Council VR. We thank ClayTech AB for supplying the clay samples.

References

[1] P.N.L. Lens, M.A. Hemminga, Nuclear magnetic resonance in environmental engineering: principles and applications, Biodegradation 9 (1998) 393–409.
[2] N. Nestle, T. Baumann, R. Niessner, Magnetic resonance imaging in environmental science, Environ. Sci. Techn. 36 (2002) 154A–160A.
[3] P. Porion, L.J. Michot, A.M. Faugere, A. Delville, Influence of confinement on the long-range mobility of water molecules within clay aggregates: a H-2 NMR analysis using spin-locking relaxation rates, J. Phys. Chem. C 111 (2007) 13117–13128.
[4] P. Porion, L.J. Michot, A.M. Faugere, A. Delville, Structural and dynamical properties of the water molecules confined in dense clay sediments: a study combining H-2 NMR spectroscopy and multiscale numerical modeling, J. Phys. Chem. C 111 (2007) 5441–5453.
[5] D.E. Woessner, B.S. Snowden Jr., A study of the orientation of adsorbed water molecules on montmorillonite clays by pulsed NMR, J. Colloid Interface Sci. 30 (1969) 54–68.
[6] J. Grandjean, P. Laszlo, Deuterium and oxygen-17 nuclear-magnetic-resonance of aqueous clay suspensions, Magn. Reson. Imag. 12 (1994) 375–377.
[7] A. Delville, J. Grandjean, P. Laszlo, Order acquisition by clay platelets in a magnetic-field. NMR study of the structure and microdynamics of the adsorbed water layer, J. Phys. Chem. 95 (1991) 1383–1392.
[8] Y. Nakashima, H_2O self-diffusion coefficient of water-rich MX-80 bentonite gels, Clay Miner. 41 (2006) 659–668.
[9] Y. Nakashima, Pulsed field gradient proton NMR study of the self-diffusion of H_2O in montmorillonite gel: Effects of temperature and water fraction, Am. Miner. 86 (2001) 132–138.
[10] T. Takahashi, T. Ohkubo, Y. Ikeda, Montmorillonite alignment induced by magnetic field: evidence based on the diffusion anisotropy of water molecules, J. Colloid Interface Sci. 299 (2006) 198–203.
[11] E.N. de Azevedo, M. Engelsberg, J.O. Fossum, R.E. de Souza, Anisotropic water diffusion in nematic self-assemblies of clay nanoplatelets suspended in water, Langmuir 23 (2007) 5100–5105.
[12] A.J. Fagan, N. Nestle, D.J. Lurie, Continuous wave MRI diffusion study of water in bentonite clay, Magn. Reson. Imag. 23 (2005) 317–319.
[13] O. Karnland, S. Olsson, U. Nilsson, Mineralogy and sealing properties of various bentonites and smectite-rich clay materials, Report SKB TR-06-30, Svensk Kärnbränslehantering AB, www.skb.se, Stockholm, 2006.
[14] S. Emid, J.H.N. Creyghton, High-resolution NMR imaging in solids, Physica B 128 (1985) 81–83.
[15] P. Bendel, M. Davis, E. Berman, G.W. Kabalka, A method for imaging nuclei with short T_2 relaxation and its application to boron-11 NMR imaging of a BNCT agent in an intact rat, J. Magn. Reson. 88 (1990) 369–375.
[16] S. Gravina, D.G. Cory, Sensitivity and resolution of constant-time imaging, J. Magn. Reson. B 104 (1994) 53–61.
[17] K. Deka, B. MacMillan, G.R. Ziegler, A.G. Marangoni, B. Newling, B.J. Balcom, Spatial mapping of solid and liquid lipid in confectionery products using a 1D centric SPRITE MRI technique, Food Res. Int. 39 (2006) 365–371.
[18] K. Deka, M.B. MacMillan, A.V. Ouriadov, I.V. Mastikhin, J.J. Young, P.M. Glover, G.R. Ziegler, B.J. Balcom, Quantitative density profiling with pure phase encoding and a dedicated 1D gradient, J. Magn. Reson. 178 (2006) 25–32.
[19] S.D. Beyea, B.J. Balcom, P.J. Prado, A.R. Cross, C.B. Kennedy, R.L. Armstrong, T.W. Bremner, Relaxation time mapping of short T-2* nuclei with single-point imaging (SPI) methods, J. Magn. Reson. 135 (1998) 156–164.
[20] Y. Nakashima, F. Mitsumori, H_2O self-diffusion restricted by clay platelets with immobilized bound H_2O layers: PGSE NMR study of water-rich saponite gels, Appl. Clay Sci. 28 (2005) 209–221.
[21] T. Ohkubo, H. Kikuchi, M. Yamaguchi, An approach of NMR relaxometry for understanding water in saturated compacted bentonite, Phys. Chem. Earth 33 (2008) S169–S176.